Int J Adv Manuf Technol (2016) 86:2197–2217
DOI 10.1007/s00170-015-8312-7

ORIGINAL ARTICLE

Experimental study on a novel minimization method of top burr formation in micro-end milling of Ti-6Al-4V

Jun Cheng[1] · **Yang Jin**[1] · **Jun Wu**[1] · **Xuelong Wen**[1] · **Yadong Gong**[1] · **Jiashun Shi**[1] · **Guangqi Cai**[1]

Received: 14 September 2015 / Accepted: 28 December 2015 / Published online: 20 January 2016

Abstract This paper investigates the top burr formation mechanism and minimization method in the micro-end milling of titanium alloy Ti-6Al-4V. The top burr formation procedure has been systematically deduced to reveal the reason for the occurrence of a top burr considering the cutting trajectory of the micro-milling tool, the chip thickness h, and the variation in the micro-milling force F_p. A new method to minimize the top burr in micro-end milling of Ti-6Al-4V is proposed in this study: resin coating is fabricated to control and reduce the top burr size by absorbing the W_p energy. A series of micro-end milling experiments were performed to test this new method. The experimental measurement results prove that the method in this study significantly reduces the top burr size in the micro-end milling of Ti-6Al-4V. Two different top burr formation modes during micro-end milling have been found, and the effect of the minimum chip thickness h_m on the top burr size is revealed. When h is below h_m, large squeezing and tearing result in a poor surface and large top burrs; when h is above h_m, the top burr size suddenly decreases. The relations between the top burr size variation b_l, b_w, and the cutting-force work W_p are determined and discussed. Based on the new technology that this study develops, a series of micro-milling surfaces with the smallest top burr size to date worldwide are achieved. The knowledge obtained from this study is expected to be an important contribution to top burr minimization in micro-machining.

✉ Jun Cheng
jcheng@mail.neu.edu.cn

[1] Advanced Manufacturing Institute, Northeastern University, P.O.Box 319, 110004 Shenyang, People's Republic of China

Keywords Micro-end milling · Top burr minimization · Resin coating · Minimum chip thickness h_m · Ti-6Al-4V

1 Introduction

Titanium base alloys such as Ti-6Al-4V are widely used for aircraft structures and turbine blades because of their high strength and low weight. In particular, due to its biocompatibility and corrosion resistance, this material is also selected to create special-shaped surfaces and structures for mostly micro-structural medical implants [1]. Despite these advantages, some defects remain in its micro-machining application. In addition to the disadvantage of being difficult to cut [2], which is a limitation to the usage of a cutting tool, the comparatively large burr is a major problem in the micro-machining of Ti-6Al-4V [3], which can cause damage and badly affect the machined surface. For conventional machining, there are some burr removal technologies [4], but most of these deburring technologies affect the machined surface.

As an important solution to achieve micro-structures, micro-end milling has a high material removal rate and wide adaptation to different materials [5]. This method has attracted increasing interest from researchers worldwide. The diameter of the manufactured micro-milling tool is 10–500 μm [6–8], and the material removal mechanism in micro-end milling of metals and alloys has been investigated. However, compared with conventional machining, the micro-milling of metals such as aluminium alloy and titanium alloy leaves large burrs on the machined surfaces. These burrs, particularly the top burrs, will certainly cause a large problem regarding the function of micro-structural components. Gillespie detected four basic burr formation mechanisms, as shown in Fig. 1a [9]. The tear burr is caused by material tearing loose from the substrate. The Poisson burr is caused by the tendency of the material to bulge

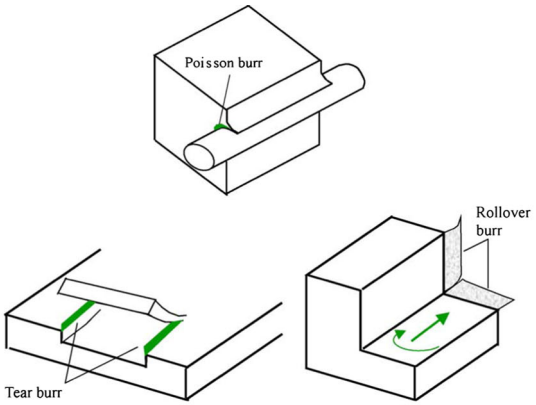

(a) Schematic of burr formation[9]

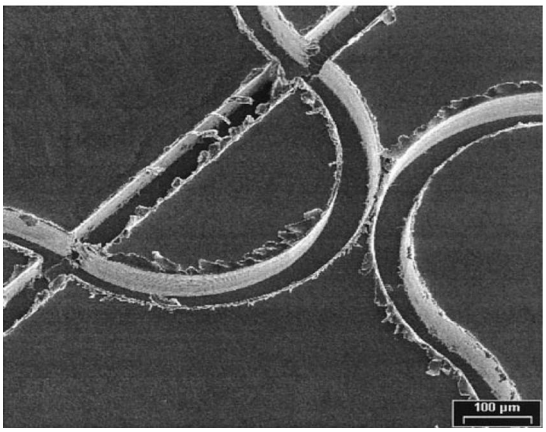

(b) Top burrs on a long groove of brass (d_s=45 μm)[10]

Fig. 1 Top burrs during micro-end milling

to the sides when it is compressed. The rollover burr, which always has a large dimension, is caused by a chip's bending instead of shearing during cutting. Schaller [10] tested a long grove with a width of less than 50 μm on brass by micro-end milling, as shown in Fig. 1b and found large top burrs on the micro-slot side. He selected electrochemical polishing as the deburring method, which provided a better burr size result, but the machined surface suffered a height loss of 2 μm.

Dornfeld [11] investigated the micro-burr formation in the micro-milling of stainless steel 304. He built a model that included the effect of the feed and cutting speed to predict and control the burr size with an accuracy of approximately ±15 %. In fact, the burr size is controlled and minimized by sacrificing the processing rate. Aurich [12] performed micro-milling experiments of Ti-6Al-4V with 48-μm micro-end mills. Burrs in up-milling and down-milling at the sides were observed and compared. Chern [13] observed five types of burrs during the milling experiments of aluminum alloy, namely, knife-type burr, wave-type burr, curl-type burr, edge breakout, and secondary burr, which is a step forward from the previous definition [9]. A valuable discovery is his proposed variation of burr size along the cylindrical edge, which reveals that the up- and down-milling sides have different burr sizes, but the reason for this phenomenon was not explained in detail. Chern et al. [14] also investigated burr formation in the micro-machining of Al 6061-T6 using a micro-tool, which was fabricated using micro-EDM. Other researchers also achieved good results regarding the top burr formation in micro-machining [15–22]. Tang et al. [15] investigated the burr formation mechanism in cross-connected micro-channel milling, and the occurrence of flake-like burr and curl-like burr was examined. Piquard et al. [16] observed the burr formation in the micro-end milling of two nickel-titanium shape memory alloys (SMA). The top burr should be the main form, and the feed per tooth and width of the cut have the most important effect to the determination of the burr size. Bi [18] optimized the process parameters for burrs in dry drilling, which shows the important effect of the cutting speed. Chen [19] experimentally proved that a small ratio of the axial depth of the cut to the mill radius significantly affected the reduction of top burr generation in the micro-ball end milling operation. Silva [20] proposed that the tool geometry and radial depth significantly affected the burr height. Liu [21] found that the curled radius of the exit burr played an important role on the burr height using micro-cutting experiments. Wu [22] performed a set of micro-machining experiments to investigate the material microstructure on the cutting force and burr formation in the micro-cutting of copper.

All of these works mainly focus on the results of burr formation, such as the burr types, and processing parameters to define the burr formation and determine the minimization method for micro-machining, which are undoubtedly useful and can have some effect. However, this study supposes that it is more important to analyze the reason that burr formation occurs during micro-machining. Only through this method, the fundamental method to control the burr formation size may be discovered.

This study attempts to investigate the key reason for the occurrence of a top burr and the formation procedure during micro-end milling of Ti-6Al-4V. The cutting trajectory of the micro-milling tool is modeled, by which the variation in chip thickness h and work of the micro-milling force W_p can be deduced. A top burr minimization method of a resin coating is proposed and successfully developed for the micro-end milling of Ti-6Al-4V. The experimental results of this new method show micro-milling surfaces with the smallest top burr size to date worldwide.

2 Burr formation mechanism in micro-end milling

2.1 Analysis of the reason of the occurrence of top burr

The formation of a burr during micro-end milling, which has factors such as size effect, comparatively large edge radius,

and minimum chip thickness [6], is a more difficult problem to solve than the conventional cutting. Hashimura [23] observed large wave burrs on both top sides of the micro-slot. Bissacco [24] assumed that the reason for these large top burrs was the size effect. Figure 2a shows the material removal mechanism of conventional cutting: the chip is sheared off the workpiece by F_s, and the chip is close to tool's rear face. φ is the shear angle; F_p and F_c are the force components along the horizontal and vertical directions, respectively. Figure 2b is the orthogonal cutting process in micro-end milling, where r is the radius of the cutting edge and h is the feed per tooth, which is almost equal to the chip thickness. From the experimental results of this study, the approximate minimum chip thickness h_m is verified to be 20 % of r. The top burr formation also has a sudden change in this range.

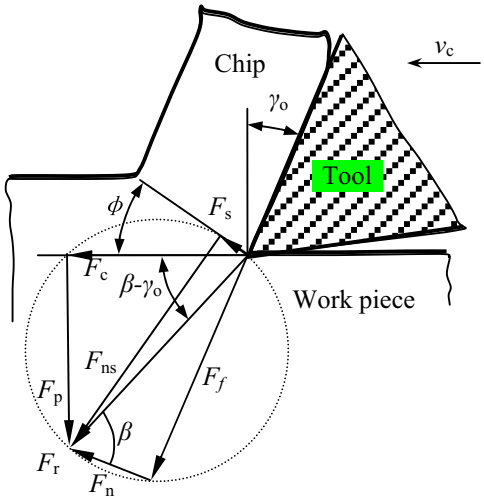

(a) Conventional cutting

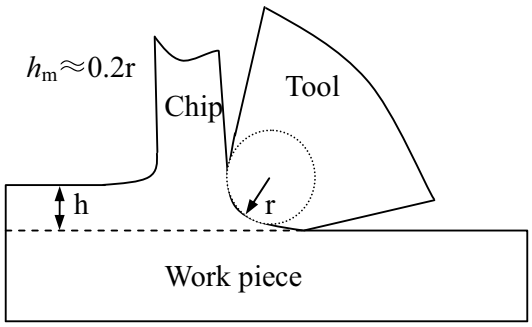

(b) Orthogonal cutting process in micro-end milling

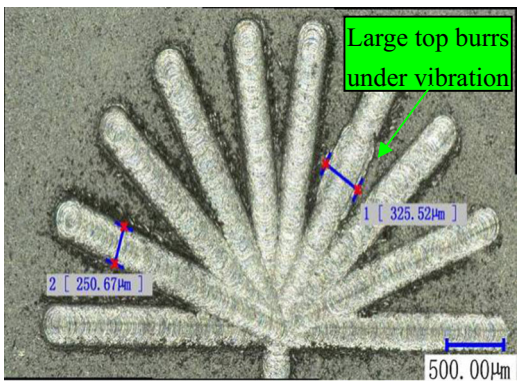

(c) Sudden change in top burrs caused by vibration

Fig. 2 Origin cause analysis of the top burr formation in micro-end milling

In micro-machining, because of the small feed per tooth and size effect, the cutting condition is changed.

To determine what causes the large bent of chips, it is essential to analyze the force condition in micro-end milling. As shown in Fig. 2a, the cutting force F_r can be deduced as follows:

$$F_r = \frac{F_s}{\cos(\phi+\beta-\gamma_o)} = \frac{\tau A_D}{sin\phi\cos(\phi+\beta-\gamma_o)} \quad (1)$$

The component force of F_r is shown as Eq. (2).

$$F_c = F_r\cos(\beta-\gamma_o);\ F_p = F_r sin(\beta-\gamma_o) \quad (2)$$

F_c and F_p are finally expressed using the following equations:

$$F_c = \frac{kha_p\cos(\beta-\gamma_o)}{\sin\phi\cos(\phi+\beta-\gamma_o)} \quad (3)$$

$$F_p = \frac{kha_p\sin(\beta-\gamma_o)}{\sin\phi\cos(\phi+\beta-\gamma_o)} \quad (4)$$

Figure 2c is a test for different direction feeds on the micro-machine. When there is a vibration during micro-end milling, the top burrs also suddenly change compared to those formed without vibration. From this analysis, it is easy to deduce that the force F_p will have an impact function on the chip during the last phase. It is reasonable to assume that the vibration aggravates the situation of the F_p impact function on the chip.

2.2 Modeling and minimization of a top burr

Figure 3a shows the top burr formation during micro-end milling; the chip is growing under the function of forces F_c and F_p. F_c is the cutting force to propel chip growth. F_p is the force with a function to push the chip to be bent. After a chip is pushed out of the trajectory of cutting by F_p, force F_c will lead it onto the sides of slots that are finally in the top burs, which can be observed.

Thus, variation in force F_p is strongly related to h by Eq. (4). To investigate the variation in the force F_p, it is essential to model the variation of undeformed chip thickness h first. This study builds a chip thickness h model as shown in Fig. 3b considering the physics relation during the entire cutting process. This model is more precise than the currently available ones.

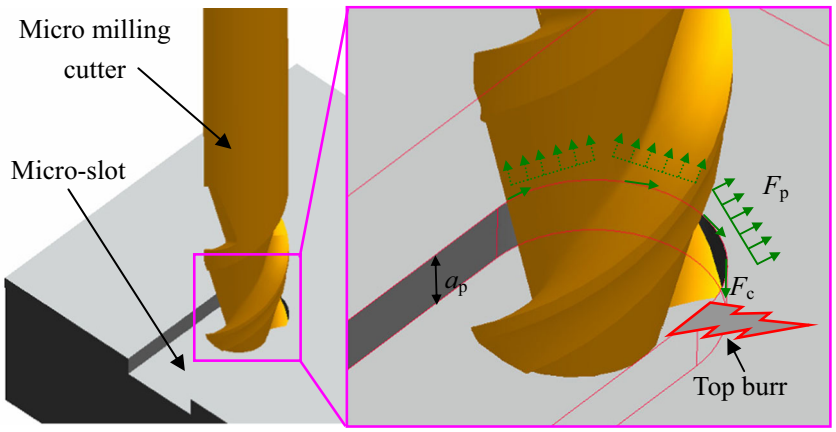

(a) Top burr formation in micro-end milling

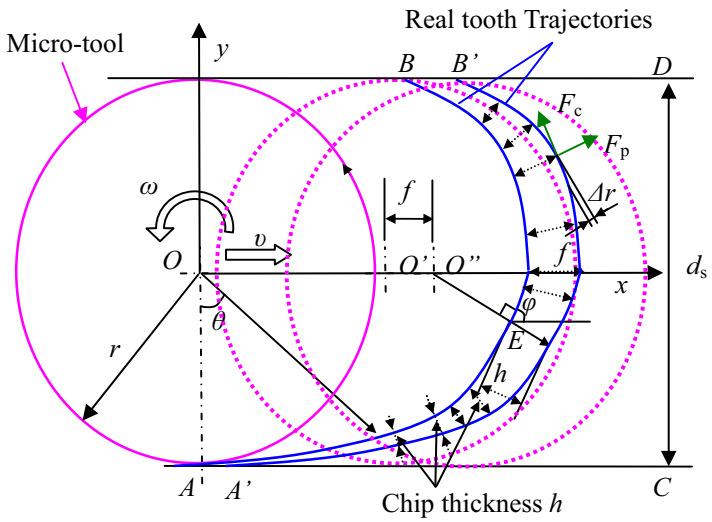

(b) Chip thickness *h* variation model

Fig. 3 Top burr formation modeling during micro-end milling

In Fig. 3b, f is the feed per tooth, v is the feed speed, and ω is the rotation speed; the variation in h is determined by two adjacent tooth trajectories in micro-end milling. The displacement function of the cutting edge with time is expressed by Eq. (5).

$$\begin{cases} x(t) = vt + r\sin\omega t \\ y(t) = -r\cos\omega t \end{cases} \tag{5}$$

The differential value is as follows:

$$\tan(\varphi) = \frac{dy(t)}{dx(t)} = \frac{r\omega\sin\omega t}{v + r\omega\cos\omega t} \tag{6}$$

Then, we substituted the angle φ, and the undeformed chip thickness h is expressed by Eq. (7).

$$h = f\sin(\varphi) = f\sin\left(\arctan\left(\frac{r\omega\sin\omega t}{v + r\omega\cos\omega t}\right)\right) \tag{7}$$

Finally, the F_p force is calculated using Eq. (8).

$$F_p = \frac{ka_p f\sin(\beta-\gamma_o)}{\sin\phi\cos(\phi+\beta-\gamma_o)}\sin\left(\arctan\left(\frac{r\omega\sin\omega t}{v + r\omega\cos\omega t}\right)\right) \tag{8}$$

The top burr is easily bent when its growth enters the last phase, as shown in Fig. 4a. The function of F_p and its value curve in Fig. 4b obviously show that F_p increases when θ is from $-\pi/2$ to 0 (zone I) and decreases when θ is from 0 to $\pi/2$ (zone II). In zone I, the increasing F_p and comparatively smaller chip size cause a smaller top burr on the up-milling side. In this zone, the types of top burr are Poisson burr and small rollover burr, and the Poisson burr is the major type. In zone II, F_p begins to decrease from the peak point in Fig. 4b, and the chip loses part of the support from the micro-milling tool. At this time, large top burrs such as wave burrs begin to appear on the down-milling side, and the type is mainly rollover burr. This result can explain why the top burr on the down-milling

side is always larger than that on the up-milling side, and the top burr types are different at different edge displacements.

As previously mentioned, the size of a single top burr is random and independent of the processing parameters. However, in the entire statistic result, it is related to some physical variable.

From the previous analysis, this study selects the work of F_p during a single cycle of feed per tooth to be the measurement of top burr size. As previously mentioned, the material removal mode has a sudden change at the minimum chip thickness h_m. Therefore, F_p and W_p also have a step, which affects the top burr formation and burr size b_l and b_w, and the function is expressed in Eq. (9).

$$\begin{cases} (b_l, b_w) = f_1(W_p) & h < h_m \\ (b_l, b_w) = f_2(W_p) & h \geq h_m \end{cases} \tag{9}$$

When h is smaller than h_m, F_p and W_p are difficult to deduce and are only achieved using an experimental regression method. When h is larger than h_m, the functions of W_p and W_c are deduced, and the differential expressions are as follows:

$$\begin{cases} dW_p = F_p d\Delta r \\ dW_c = F_c d\Delta l \end{cases} \tag{10}$$

The operating distances Δr and Δl are solved using Eqs. (11) and (12).

$$d\Delta r = r\cos\theta d\theta = rw\cos(wt)dt \tag{11}$$

$$d\Delta l = rd\theta = rwdt \tag{12}$$

After substituting F_p and F_c, the final expressions of W_p and W_c are as follows:

$$W_p = \int_{-\pi/2}^{\pi/2} F_p r\cos\theta d\theta = \int_0^{\pi/\omega} \frac{r\omega k f a_p \sin(\beta-\gamma_o)}{\sin\phi\cos(\phi+\beta-\gamma_o)} \sin\left(\arctan\left(\frac{r\omega\sin\omega t}{v+r\omega\cos\omega t}\right)\right)\cos\omega t dt \tag{13}$$

$$W_c = \int_{-\pi/2}^{\pi/2} F_c r d\theta = \int_0^{\pi/\omega} \frac{r\omega k f a_p \cos(\beta-\gamma_o)}{\sin\phi\cos(\phi+\beta-\gamma_o)} \sin\left(\arctan\left(\frac{r\omega\sin\omega t}{v+r\omega\cos\omega t}\right)\right) dt \tag{14}$$

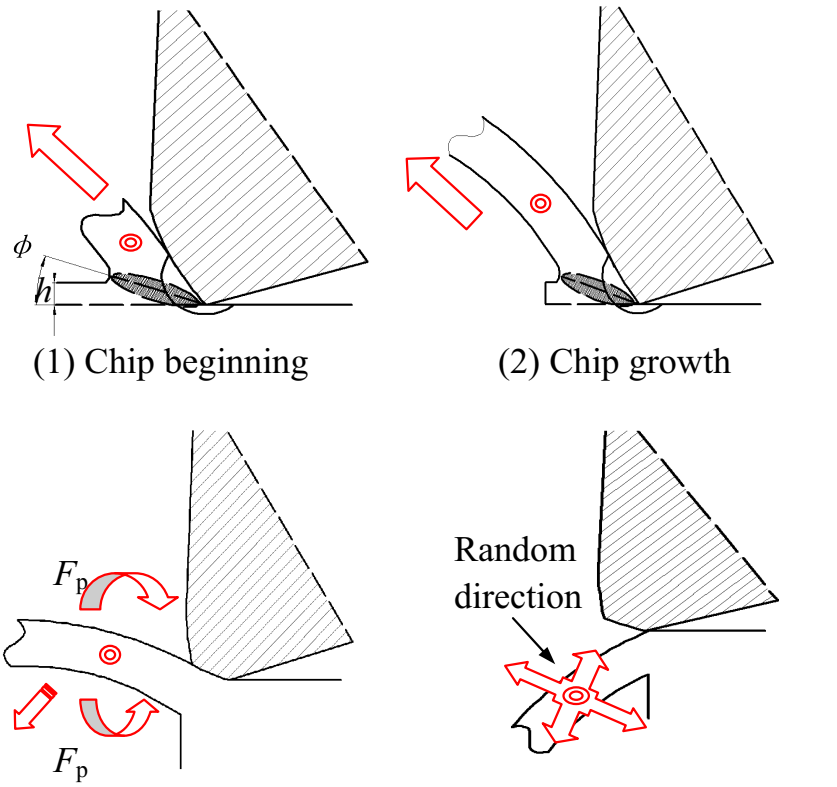

Fig. 4 Models of top burrs in micro-end milling

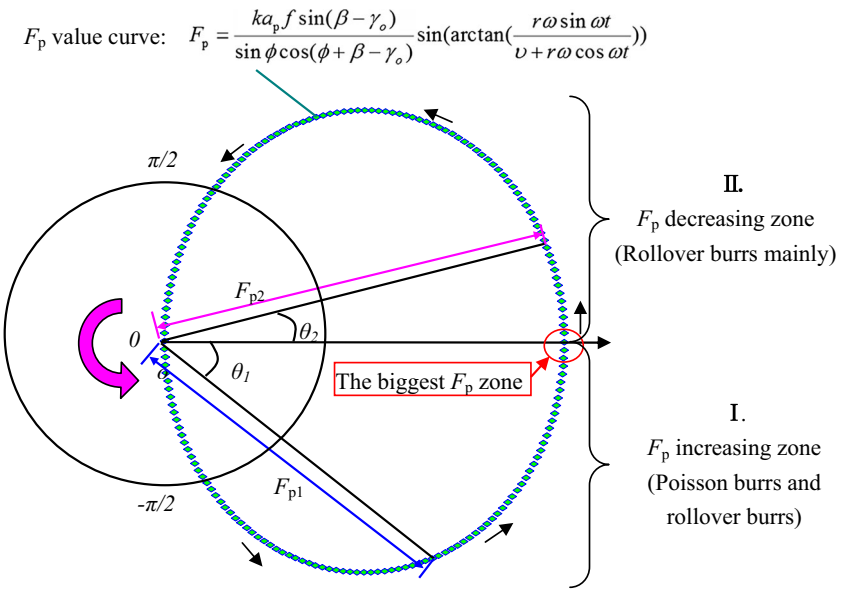

(b) F_p model considering the h variation

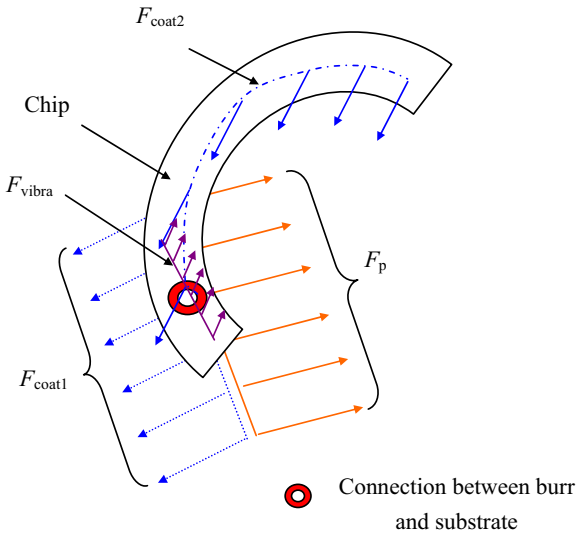

(c) Mechanical condition of a top burr

Fig. 4 (continued)

The empirical formula of the top burr length b_l based on the proposed theory in this study is expressed by Eq. (15), where k is the rake ratio coefficient and b_c is the intercept coefficient.

$$b_l = \frac{kW_p}{a_p} + b_c \tag{15}$$

On the up-milling side, the top burr length model Eq. (15) is expressed as follows:

$$b_{lu} = \frac{kW_p}{a_p} + b_{cu}(\text{up-milling}) \tag{16}$$

On the down-milling side, the top burr length model Eq. (15) is expressed as follows:

$$b_{ld} = \frac{kW_p}{a_p} + b_{cd}(\text{down-milling}) \tag{17}$$

As previously mentioned, the top burr formed during micro-machining is comparatively larger than that formed during conventional machining. Moreover, the available deburring methods such as electrochemical polish are time-consuming and cause damage to the machined surface. The previous paragraph has illustrated

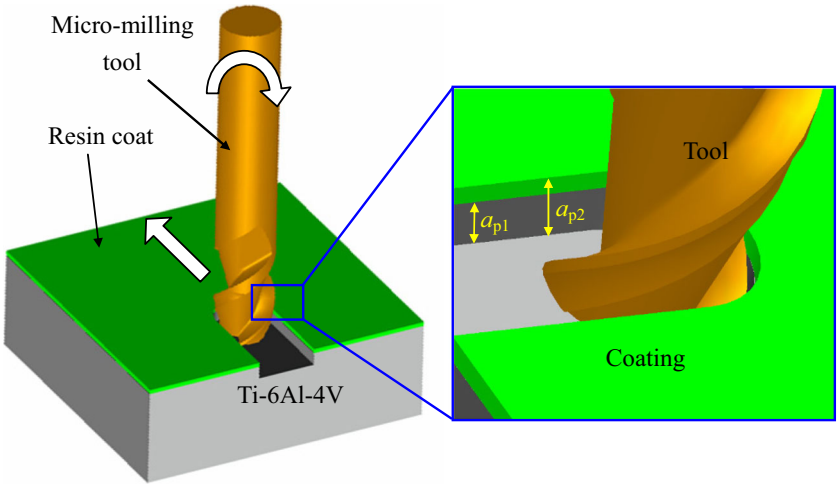

Fig. 5 Top burr minimization method with a resin coating

that top burr formation and its variation in the micro-end milling of Ti-6Al-4V are strongly affected by the variation in F_p work. To some extent, the amount of W_p in Eq. (13) determines the burr size.

The mechanical condition of the top burr is shown in Fig. 4c. This study proposes a new burr minimization technology based on this theory. First, a thin epoxy resin layer is coated onto the surface of the workpiece. This resin coating

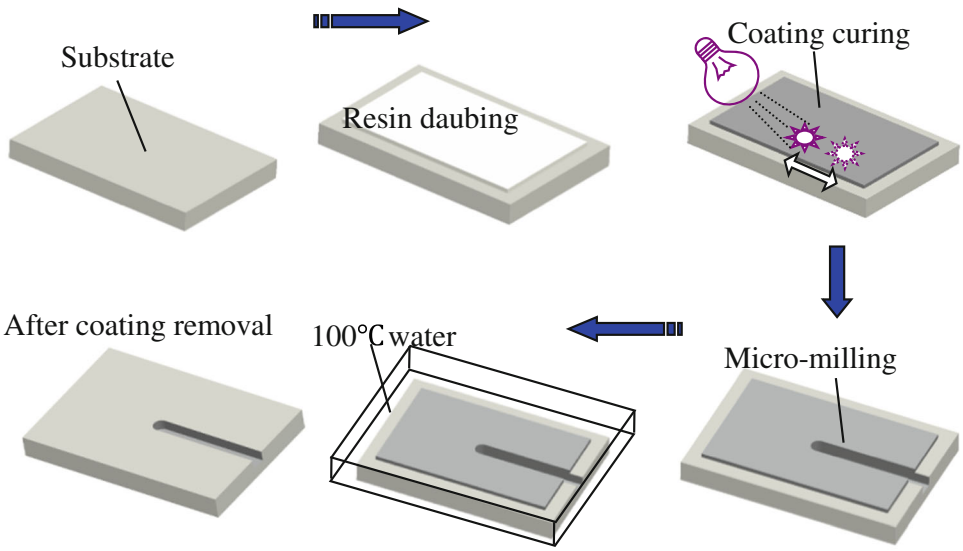

(a) Coating fabrication process

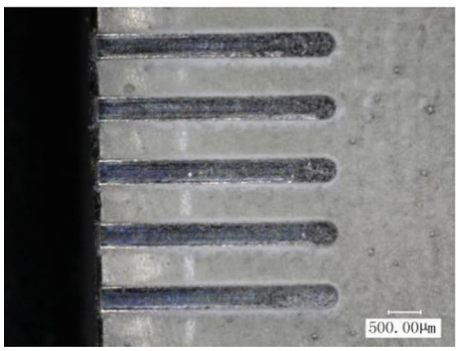

(b) Micro-slots after micro-milling

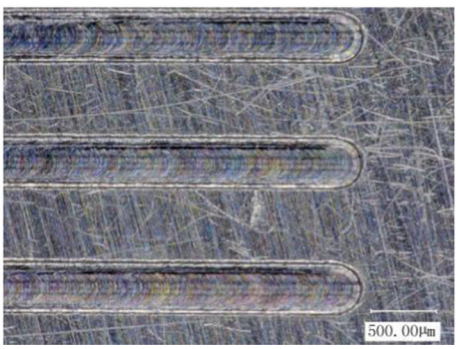

(c) Micro-slots after coating removal

Fig. 6 Fabrication procedure of the resin coating for top burr minimization

Table 1 Basic attributes of the resin coating

Property	Value
Shear strength τ (MPa)	18
Density ρ (g/cm^3)	1.18
Modulus of elasticity E (MPa)	2490
Thermal range T (°C)	−60~100
Coating thickness h_c (mm)	0.5

provides the additional holding forces F_{coat1} and F_{coat2}, which can absorb the work of F_{p} at the feed direction, hold the chip, and prevent it from bending in the depth direction.

$$b_{l-coating} = \frac{k\left[W_{\text{p}} - \pi^{1/2}(F_{coat1} + F_{coat2})c^{1/2}\right]^r}{a_p} + b_{c-coating} \quad (18)$$

Considering the absorbing effect of the resin coating, the expression of the top burr size with this new technology is deduced in Eq. (18), where c is the resin crack dimension and $b_{\text{l-coating}}$ and $b_{\text{c-coating}}$ are the burr size and intercept coefficient, respectively.

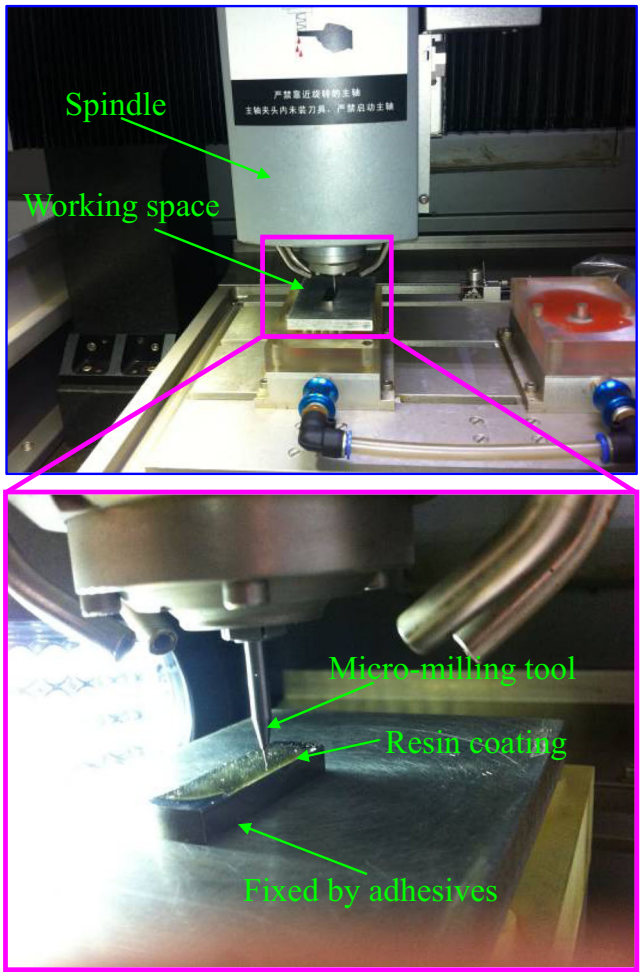

Fig. 7 Micro-machining tool and coating-assisted micro-end milling

Table 2 Machining conditions of the micro-end milling experiments

Factors	Value
Number of flutes	2
Spindle rotation speed (rpm)	60,000
Tool diameter d_s (μm)	400
Axial cutting depth a_{p} (μm)	20, 50
Feed per tooth f (μm)	0.05, 0.2, 0.5, 1, 1.5, 2, 2.5, 3, 3.5, 4, 4.5, 5
Coolant (yes or no)	No

Finally, a new burr minimization method for the micro-end milling of Ti-6Al-4V with a resin coating is shown in Fig. 5. The axial cutting depth a_{p} is changed from a_{p1} to a_{p2}. Several experiments were performed to test the function of this new technology.

3 Experimental setup

3.1 Fabrication of resin coating

The detailed fabrication process of a resin coating is shown in Fig. 6a. First, the resin was daubed on the Ti-6Al-4V substrate, and the coating thickness was controlled. Then, the resin was solidified by curing. After the coating curing process, a micro-milling experiment for the top burr investigation was begun.

Because of the liquid attribute of resin, the resin could be daubed onto a complex surface before coating curing. Therefore, using this new coating method, different surfaces and even 3D surfaces can be coated to minimize the top burr before micro-machining. Importantly, the curing equipment is ultraviolet, so the surface to be machined must have a means for exposure to the light source. The light source in this study was UV curing light, whose power was 160 W, and the exposure time was 3 min.

After the micro-milling experiments in Fig. 6b, the resin coating, which finished its top burr minimization task, could be removed by steeping in hot water for 5 min. The final micro-milling slots using this technology are shown in Fig. 6c. The basic attributes of the resin coating are listed in Table 1.

Table 3 Basic attributes of Ti-6Al-4V

Properties	Value
Tensile strength σ_b (MPa)	902
Yield strength σ_s (MPa)	824
Density ρ (g/cm^3)	4.5
Modulus of elasticity E (GPa)	105
Elongation δ (%)	10

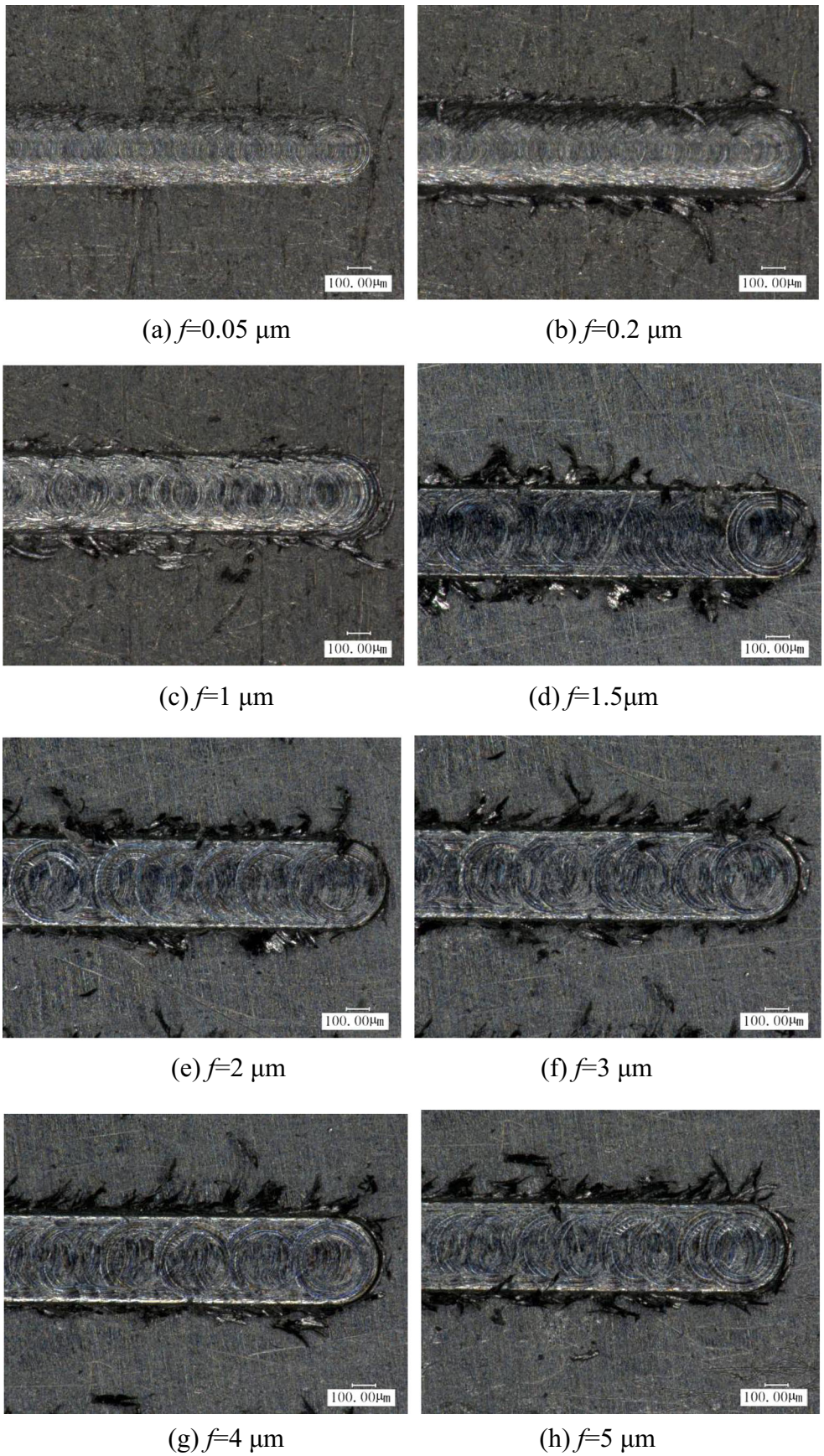

(a) f=0.05 μm (b) f=0.2 μm

(c) f=1 μm (d) f=1.5μm

(e) f=2 μm (f) f=3 μm

(g) f=4 μm (h) f=5 μm

Fig. 8 Uncoated micro-milling results of Ti-6Al-4V (a_p = 20 μm)

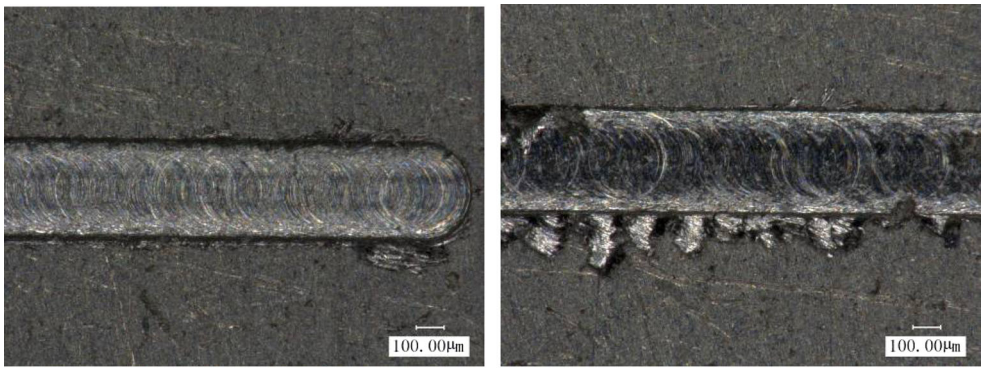

(a) f=0.05 μm (b) f=0.2 μm

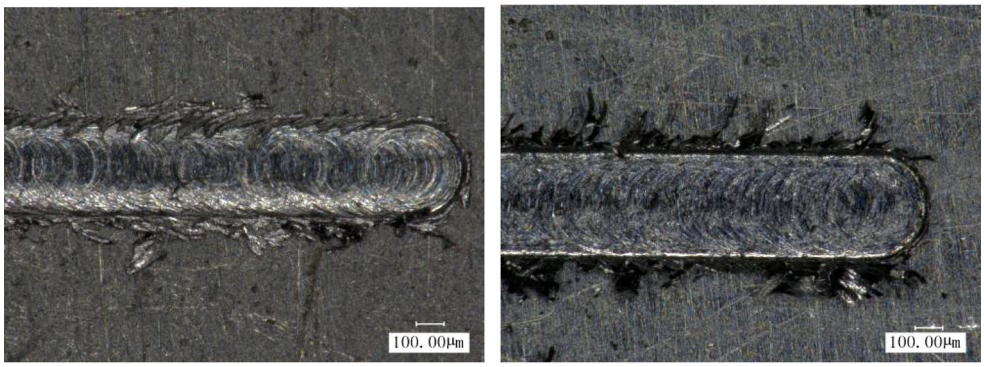

(c) f=1 μm (d) f=1.5μm

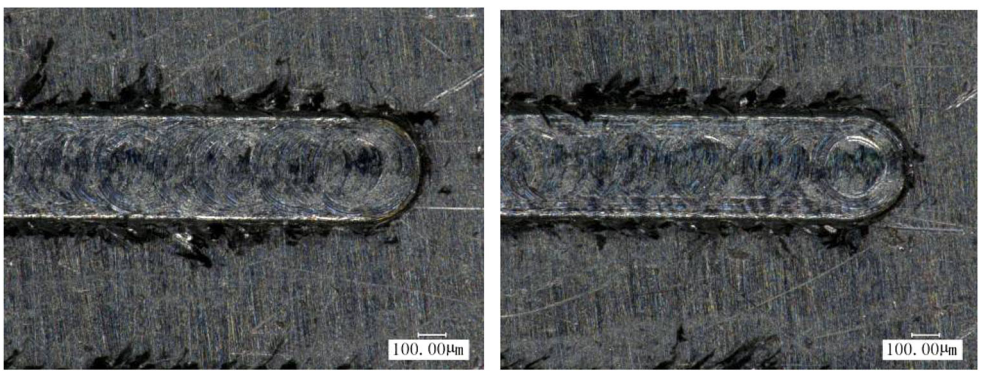

(e) f=2 μm (f) f=3 μm

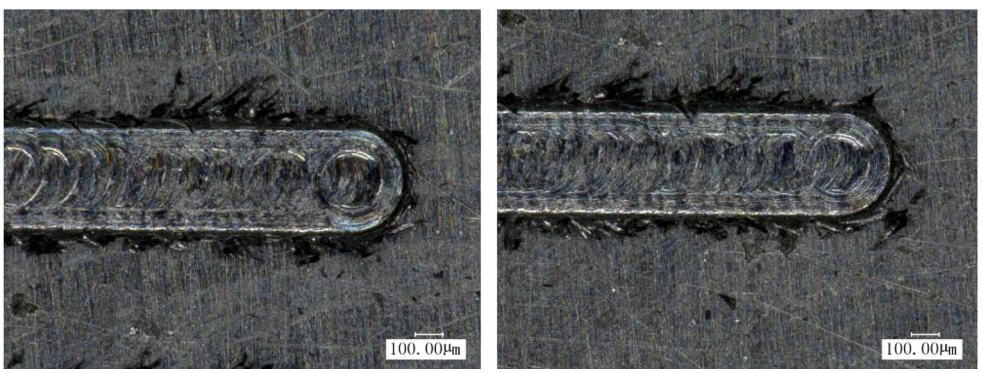

(g) f=4 μm (h) f=5 μm

Fig. 9 Uncoated micro-milling results of Ti-6Al-4V (a_p = 50 μm)

3.2 Micro-milling tool and material

The micro-end milling experiments of Ti-6Al-4V were performed on a precision micro-machine tool, as shown in Fig. 7. The tool has a 0.1-μm positioning resolution, and the rotation speed of its axis can be as high as 60,000 rpm. The micro-machining condition of the experiments in this study is listed in Table 2.

The micro-end milling tool in this study has two flutes, its diameter d_s is 400 μm, and the edge radius is less than 4 μm. The spindle rotation speed is 60,000 rpm, the selected axial cutting depth a_p is below 50 μm, and the feed per tooth f is 0.1–5 μm.

Resin debris also accumulates in the groove of the rear face of the tool as shown in Fig. 9e, which has a weak jamming effect in the chip groove. Therefore, the micro-milling tool that is used under a resin coating must be cleared at regular intervals, and this requirement is a limitation of this technology.

In the detailed view of Fig. 7, the working space of the experiment and coating for burr minimization are shown. The epoxy resin coating, which was fabricated in this study, minimized the top burr. The workpiece in the experiment was made of titanium alloy Ti-6Al-4V, and its basic attributes are listed in Table 3.

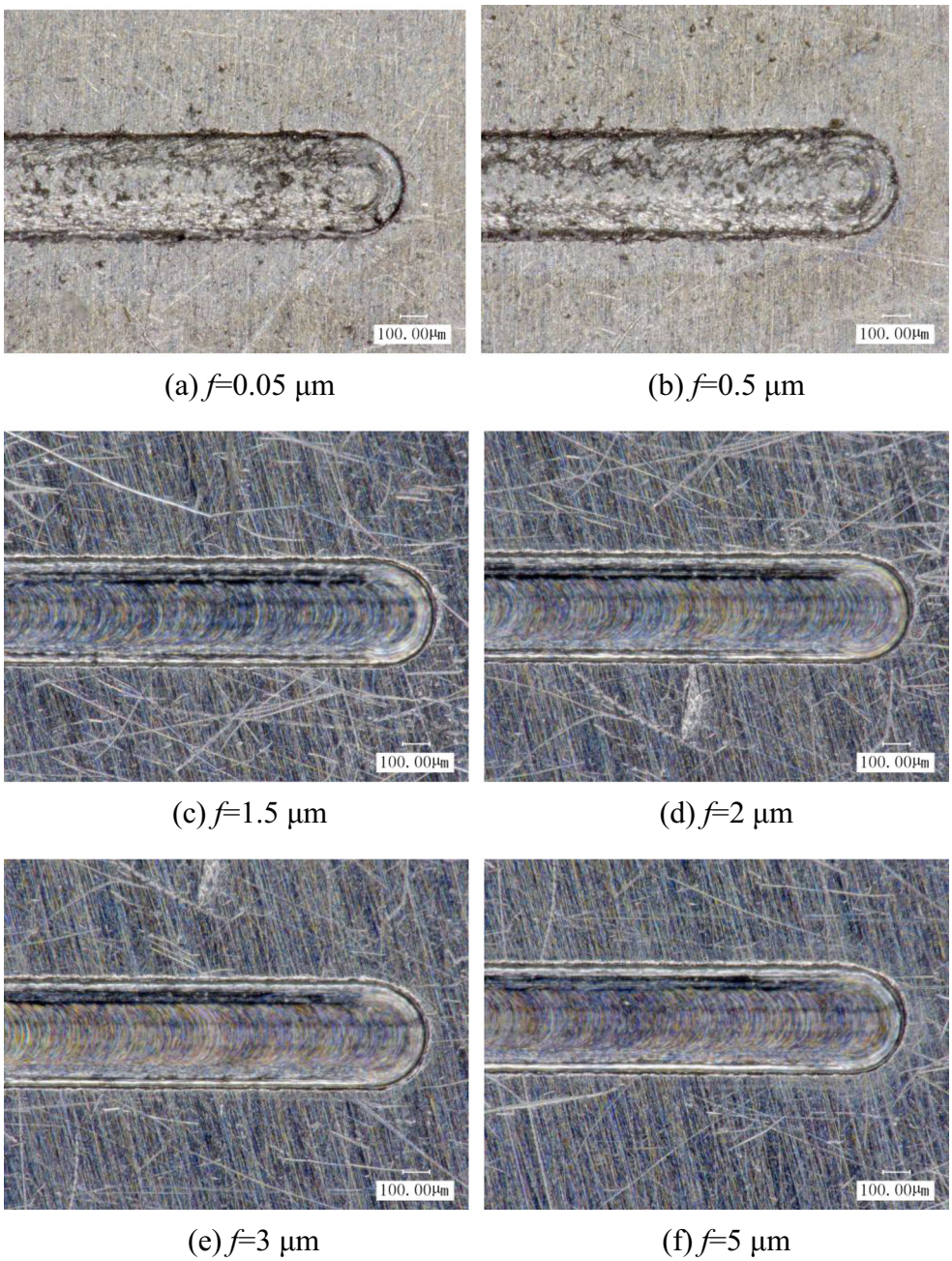

(a) f=0.05 μm (b) f=0.5 μm

(c) f=1.5 μm (d) f=2 μm

(e) f=3 μm (f) f=5 μm

Fig. 10 Coated micro-milling results of Ti-6Al-4V (a_p = 20 μm)

4 Results and discussion

4.1 Experimental results in micro-end milling of Ti-6Al-4V

To investigate the top burr formation mechanism and effect of the proposed and developed minimization method in this study, a series of micro-milling experiments were performed using the micro-machine tool in Fig. 7. Both uncoated and coated micro-milling methods have identical experiment parameters according to the values in Table 2. The untreated experimental results of the micro-milling of Ti-6Al-4V using the uncoated method are presented in Figs. 8 and 9. In Fig. 8, the axial cutting depth a_p is 20 μm. Figure 9 shows the results with $a_p = 50$ μm.

Figures 8 and 9 show that the top burr changes with the change in feed per tooth f. The transformation of the top burr formation appears different in different feed-per-tooth ranges. When f is small (0.05–1 μm), the maximum burr size rapidly increases and tends to be large; the type is mainly rollover burr, but wave burrs also occur in this range. When the feed per tooth f is beyond 1.5 μm, the maximum burr size appears to increase more slowly, and

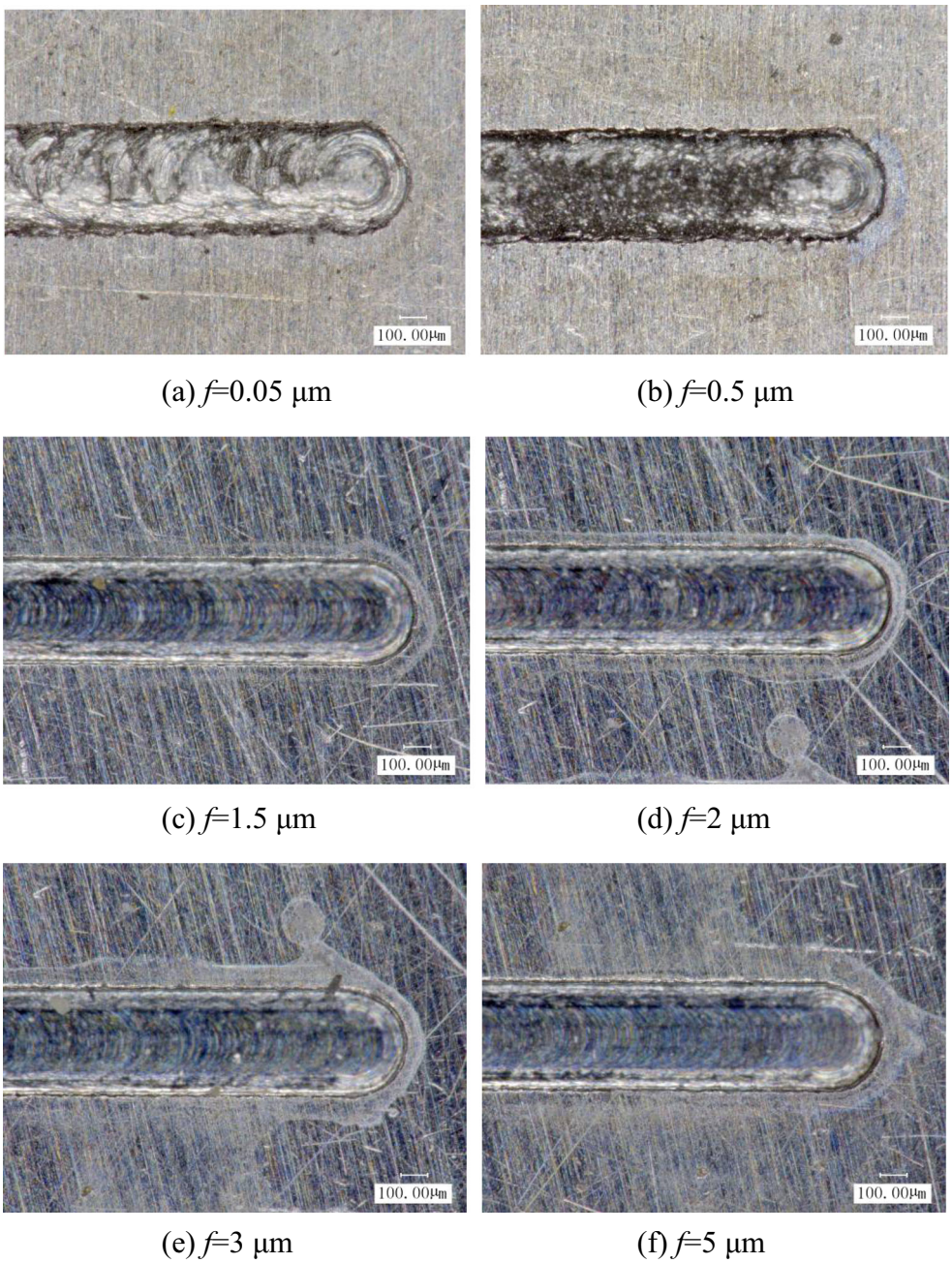

(a) f=0.05 μm (b) f=0.5 μm

(c) f=1.5 μm (d) f=2 μm

(e) f=3 μm (f) f=5 μm

Fig. 11 Coated micro-milling results of Ti-6Al-4V ($a_p = 50$ μm)

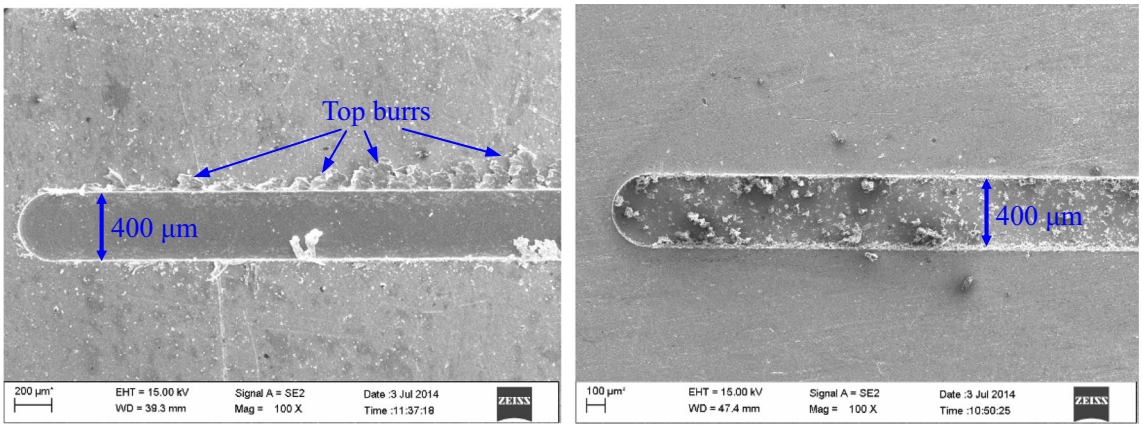

(a) Micro-slot (uncoated) (b) Micro-slot (coated)

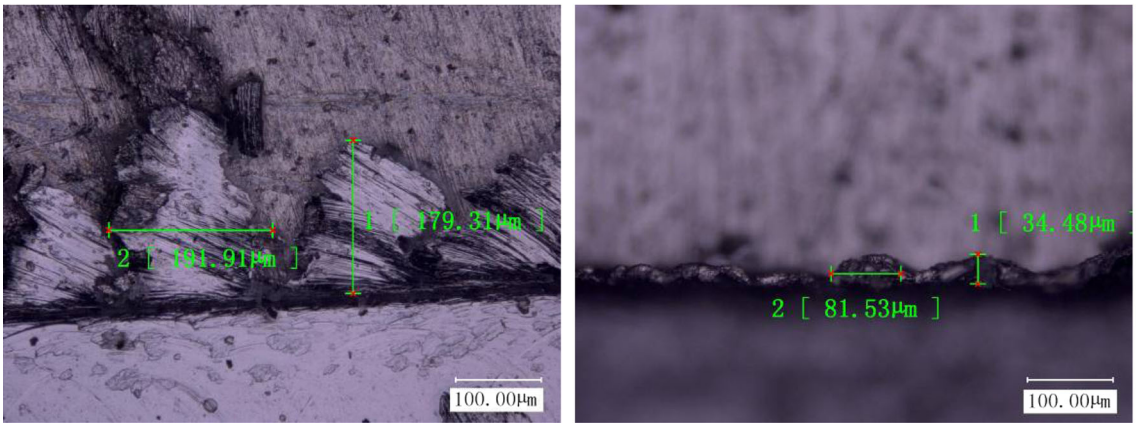

(c) Top burr size measurement (uncoated) (d) Top burr size measurement (coated)

Fig. 12 Comparison of an entire micro-milling slot (f = 0.2 μm, a_p = 50 μm)

its type changes to tear burr and is more similar to the cutting chips. Different values of the axial cutting depth a_p can affect the top burr width but do not have a significant effect on the top burr length.

Figures 10 and 11 show the experimental results of the micro-milling of Ti-6Al-4V using the coated method. The axial cutting depth a_p is 20 and 50 μm in Figs. 10 and 11, respectively. The large top burr formations such as wave burr

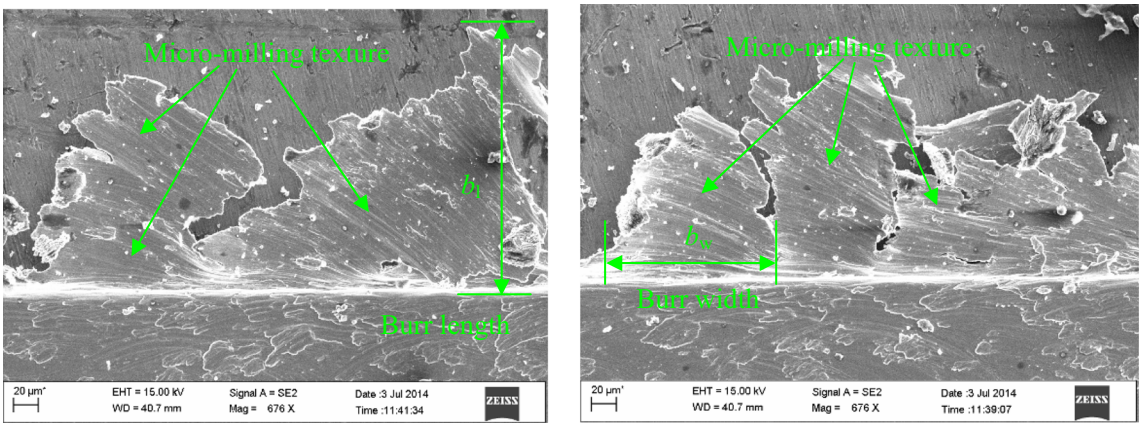

(a) Position 1# (b) Position 2#

Fig. 13 Wave top burrs in uncoated results (d_s = 400 μm; f = 0.2 μm; a_p = 50 μm)

and curl burr are effectively controlled, and the burr size is significantly reduced using this new technology.

Meanwhile, at some particular range, there is a sudden change in the top burr size. At small feeds per tooth f such as 0.05 and 0.2 μm, the top burrs are controlled to be small but remain present, and resin chips remain on the machined surface. When f is beyond 1.5 μm, there is almost no top burr on the milling side, as shown in Figs. 10c–f and 11c–f. The machined surfaces are also clearer with no resin chips. These

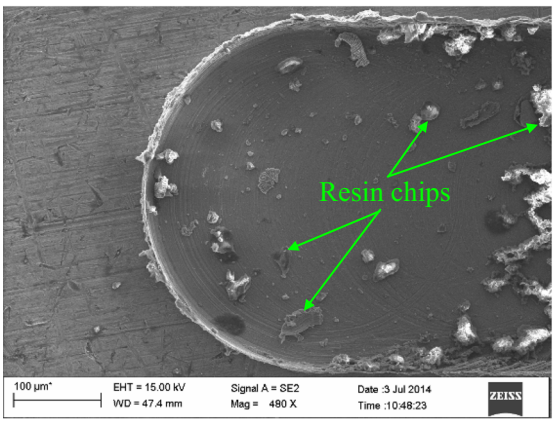

(a) f=0.2 μm, a_p=20 μm (coated)

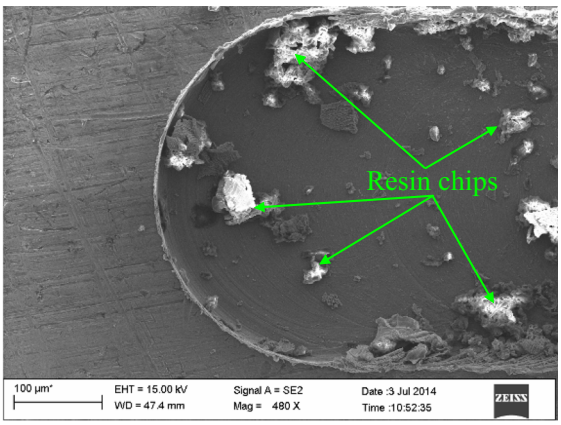

(b) f=0.2 μm, a_p=50 μm (coated)

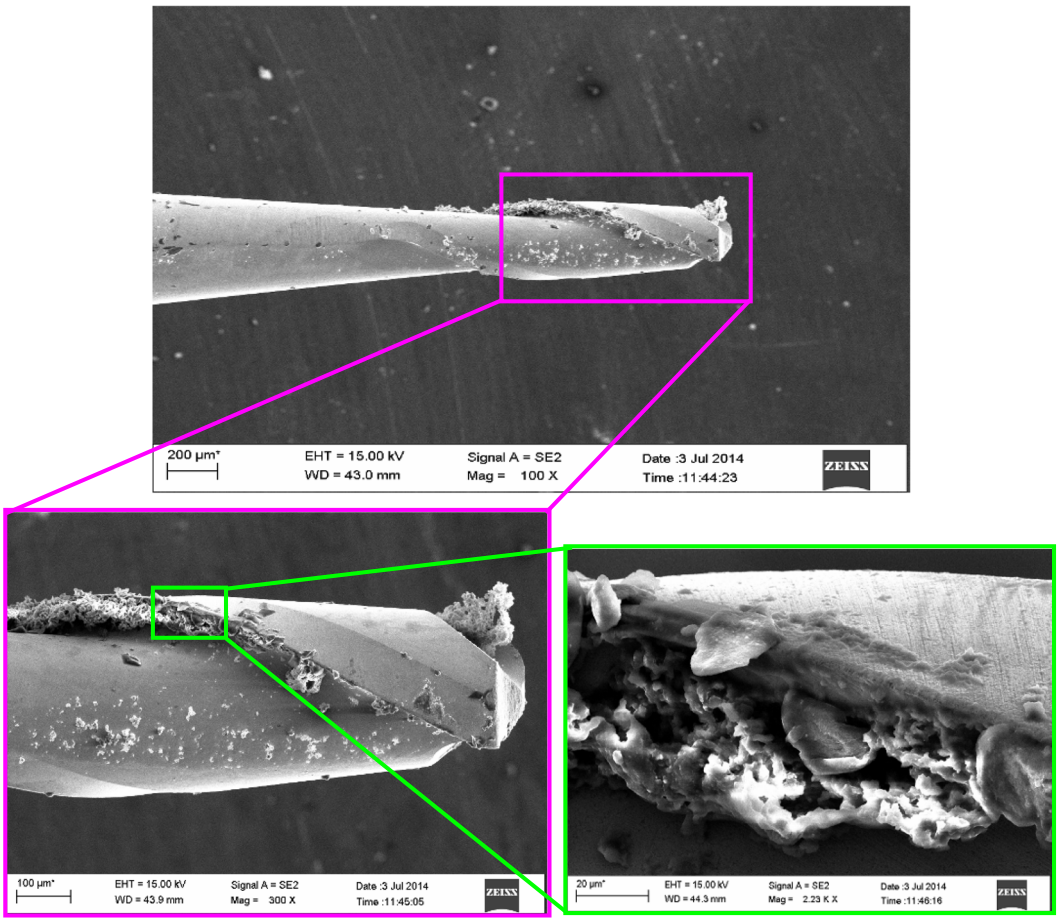

(c) Resin accumulation on the micro-milling tool

Fig. 14 Entry of the micro-milling slots of the coated results

results strongly prove the significant application value of the method in this study. In fact, these results are the precision micro-milling surface with the smallest top burr size worldwide to date.

4.2 Top burr formation under different conditions

As previously mentioned, the work of F_p along the chip thickness direction, which is W_p as analyzed in paragraph 2.2 and Eq. (13), should be the key reason for the occurrence of top burrs in this study. To verify this point and investigate the formation of top burr in micro-milling experiments, this study selects the micro-slot entry in the micro-end milling of Ti-6Al-4V to investigate in detail using a microscope and SEM scanning.

The SEM images in Fig. 12a, b are the experimental results (f = 0.2 μm, a_p = 50 μm) using different methods. Figure 12a is the uncoated result, and Fig. 12b is the coated result. Large top burrs are observed on the down-milling side of Fig. 12a, which is consistent with the relationship of the conventional top burr formation knowledge. On the contrary, no large top burr is found on the milling sides of Fig. 12b. The measured top burr size for the uncoated and coated methods are shown in Fig. 12c, d. In this study, the five largest burrs of one slot were selected to calculate and average the maximum top burr size value; both burr length and burr width values were determined using this method.

A large cutting parameter often causes large wave burrs, whose surface and texture are easily investigated, as shown in Fig. 13. The detailed observation of the top burrs in Fig. 13a, b shows that all burrs have obvious micro-milling textures on their surface. This strong evidence proves that large top burrs in the micro-end milling of Ti-6Al-4V are mainly transferred by chips, which are bent by other effects during the process. In other words, this evidence supports the point of this study in Fig. 2.

Furthermore, the slot entry situations in the micro-end milling of Ti-6Al-4V with a top burr minimization coating are shown in Fig. 14a, b. Obviously, there is no large burr formation on the slots' entry sides because the resin coating absorbs W_p. The additional holding forces F_{coat1} and F_{coat2}, which are

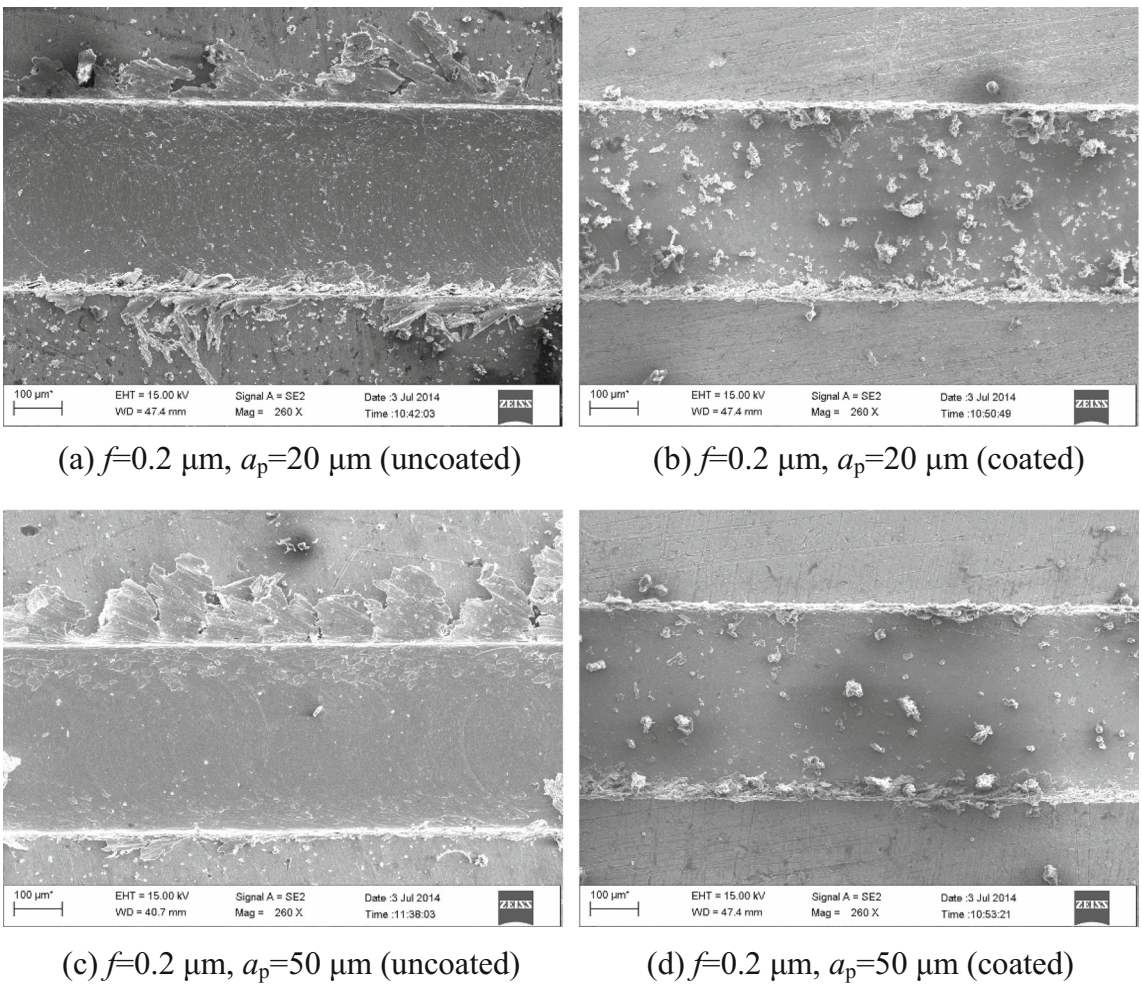

(a) f=0.2 μm, a_p=20 μm (uncoated) (b) f=0.2 μm, a_p=20 μm (coated)

(c) f=0.2 μm, a_p=50 μm (uncoated) (d) f=0.2 μm, a_p=50 μm (coated)

Fig. 15 Comparison of micro-milling slots between uncoated and coated results

provided by the resin coating, control and restrain the occurrence and formation of large top burrs. This phenomenon strongly verifies the models in Fig. 4. The remaining resin chips on the machined slot surface can be removed in a hot-water soak.

The resin debris also accumulates in the groove of the tool rear face, as shown in Fig. 14c, which has a weak jamming effect in the chip groove. Therefore, the micro-milling tool in the resin coating case must be cleared at regular intervals, which is a small limitation of this technology.

4.3 Effect of the top burr minimization method

To observe the top burr minimization process in detail, particularly in a range of small feed per tooth, the uncoated and coated micro-milling slots of the micro-end milling of Ti-6Al-4V are compared in Fig. 15. The experimental results show that the coated workpieces have better top burr results. Figure 15a, b have the cutting conditions of $f=0.2$ μm and $a_p=20$ μm. Figure 15c, d have the cutting conditions of $f=0.2$ μm and $a_p=50$ μm. Obviously, Fig. 15c shows a larger top burr size on the down-milling side than those in Fig. 15a because of the larger cutting depth. However, the coated results are almost unaffected by the cutting depth. The top burrs in Fig. 15d when a_p is 50 μm exhibit identical conditions compared to those in Fig. 15b, where a_p is 20 μm. These characteristics demonstrate that this new technology has a superior effect on top burr control during the micro-end milling of Ti-6Al-4V. Nonetheless, the SEM micrographs in Fig. 15a, c indicate that the top burrs on the down-milling side are always larger than those on the up-milling side, and the top burrs tend to be Poisson type on the up-milling side, whereas the large wave burr and curl burr belong to the rollover type. This result supports the proposed theoretical model in Fig. 4 of this study.

The experimental results when the feed per tooth f is 0.2 μm are selected to investigate and compare in Fig. 16. Different types of top burrs on the down-milling sides are observed, and their sizes, which include the aforementioned burr length and burr width, were measured. As previously discussed, a resin coating that absorbs the work of F_p introduces advantages in top burr minimization during micro-end milling of Ti-

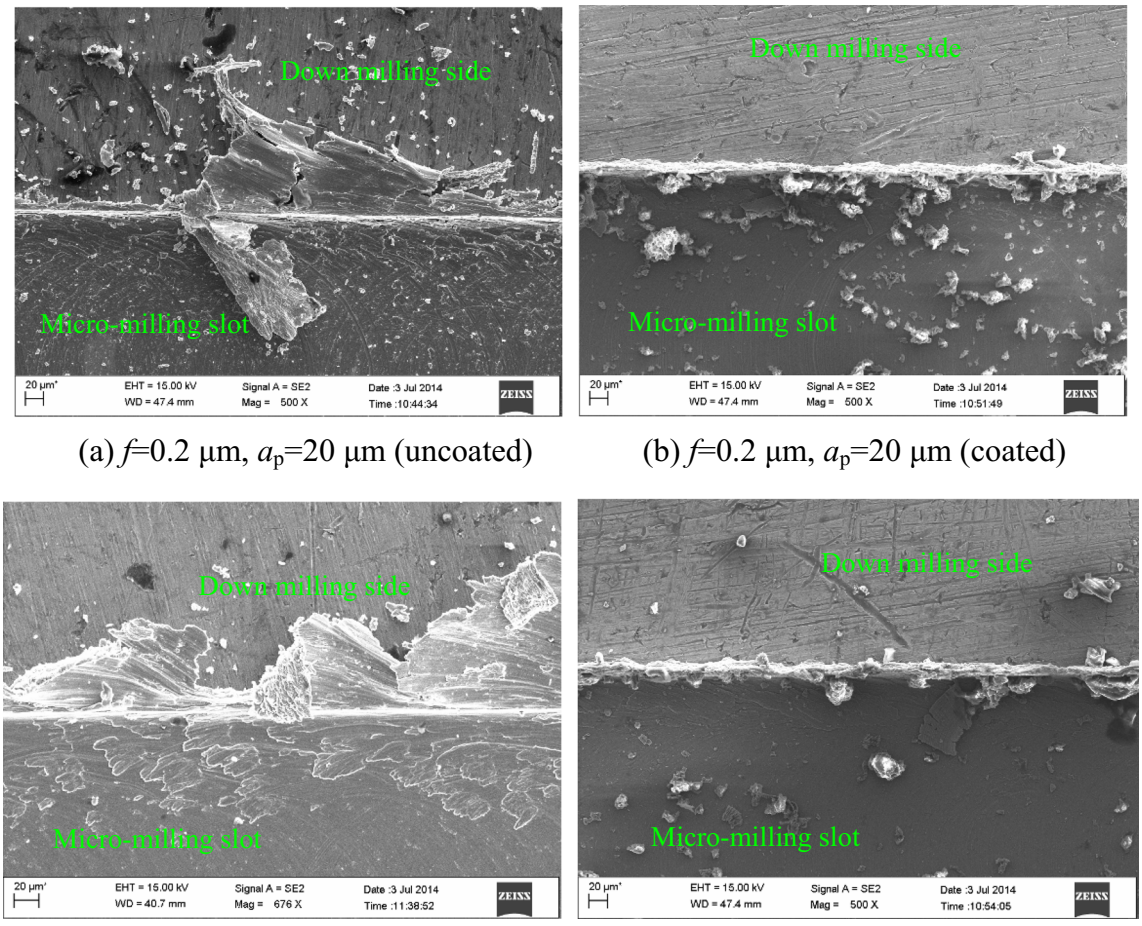

(a) f=0.2 μm, a_p=20 μm (uncoated) (b) f=0.2 μm, a_p=20 μm (coated)

(c) f=0.2 μm, a_p=50 μm (uncoated) (d) f=0.2 μm, a_p=50 μm (coated)

Fig. 16 Comparison of top burrs on the down-milling side

6Al-4V. When this resin coating minimization technology for top burr was used, a resin coating was first fabricated on the surface of the workpiece. The comparison result in Fig. 16 shows that the large top burr formation such as wave burr and curl burr were almost totally restrained using this new technology.

As mentioned in Sect. 4.1, there is a sudden change in the minimization effect of the coated method during

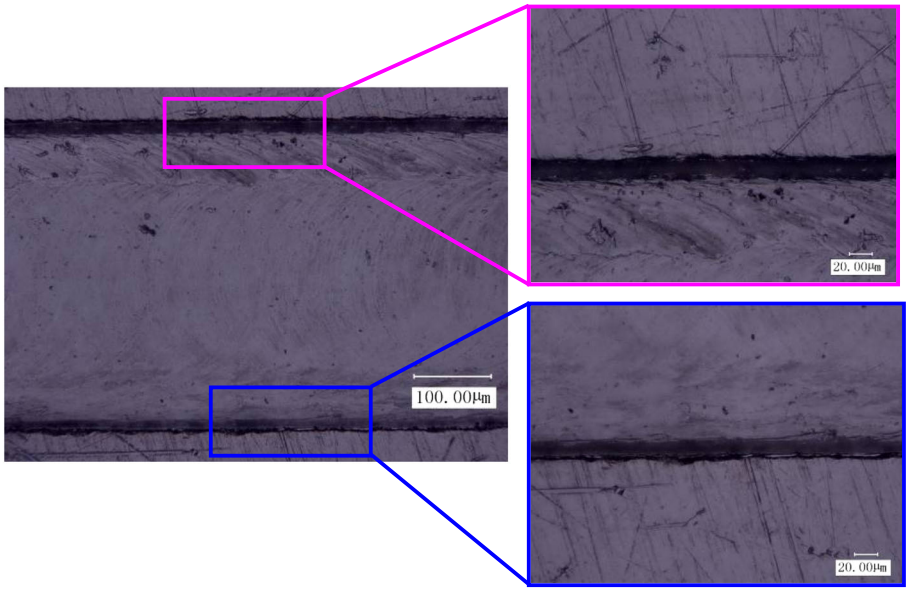

(a) Micro-slot beyond a sudden change (f=1.5 μm)

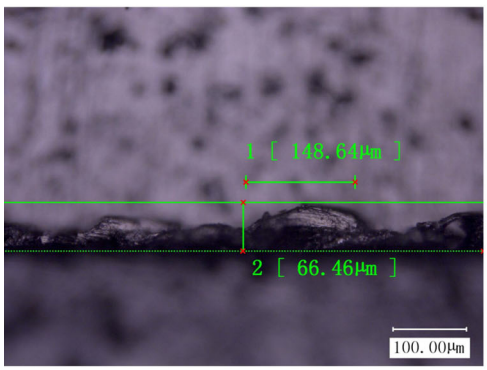

(b) f=0.5 μm (Up-milling side)

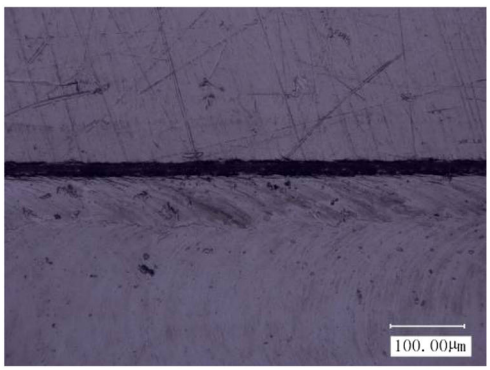

(c) f=1.5 μm (Up-milling side)

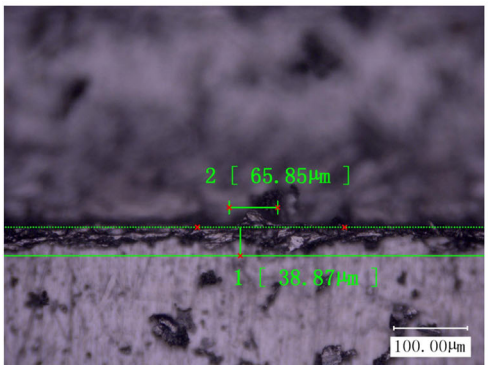

(d) f=0.5 μm (Down-milling side)

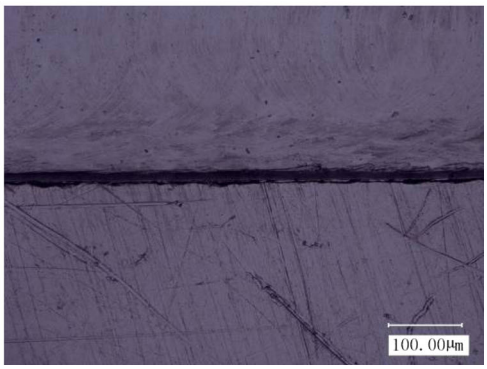

(e) f=1.5 μm (Down-milling side)

Fig. 17 A sudden change of burr minimization effect in coated results (a_p = 20 μm)

micro-end milling of Ti-6Al-4V. Figure 17a shows a micro-slot and its detailed edge views when the axial cutting depth a_p is 20 μm and the feed per tooth f is 1.5 μm. This microscope image is an untreated result of a recently finished experiment. There is almost no top burr on the milling sides, which does not induce any harm to the machined surface.

Figure 17b, c compares the top burr on the up-milling side between 0.5 and 1.5 μm of feed per tooth. Figure 17d, e shows those on the down-milling sides. There is an obvious sudden change in this range, where the top burr size suddenly decreases and even disappears. This result provides the best suitable scope of the burr minimization method that this study proposed.

To determine the reason for this phenomenon, the author analyzed the results of the material removal mechanism and the tool dimension measurements.

As known worldwide, the minimum chip thickness h_m is an important constant in micro-machining. Commonly, it is 15~20 % of the corner radius. When the cutting parameter is below h_m during micro-machining, the chip cannot be smoothly formed, and there is only squeezing and ploughing of the material. In the experimental results of this study, the sudden changes also occur in that range. This coincidence, which caught the author's attention, is interesting and important to the top burr minimization effect of the new method, which this study proposed. Therefore, to determine the precise corner radius r and minimum chip thickness h_m, the micro-milling tool after the experiments was measured in detail, and the results are shown in Fig. 18. The radius values of two cutting blades are 7.46 and 8.54 μm.

4.4 Analysis of top burr size variation

In this study, h_m was calculated to be approximately 1.5 μm based on the measurement of the corner radius in Fig. 18. In this range, the feed per tooth f is treated as equal to the chip thickness h. Figures 19 and 20 show the burr size variation of both coated results and uncoated results on the up- and down-milling sides. Both the burr length b_l and the burr width b_w decrease when the feed per tooth f crosses the minimum chip thickness h_m. The burr sizes of the coated results obviously decrease to zero when f crosses 1.5 μm. Therefore, the change in the material removal mode leads to the decrease in burr size.

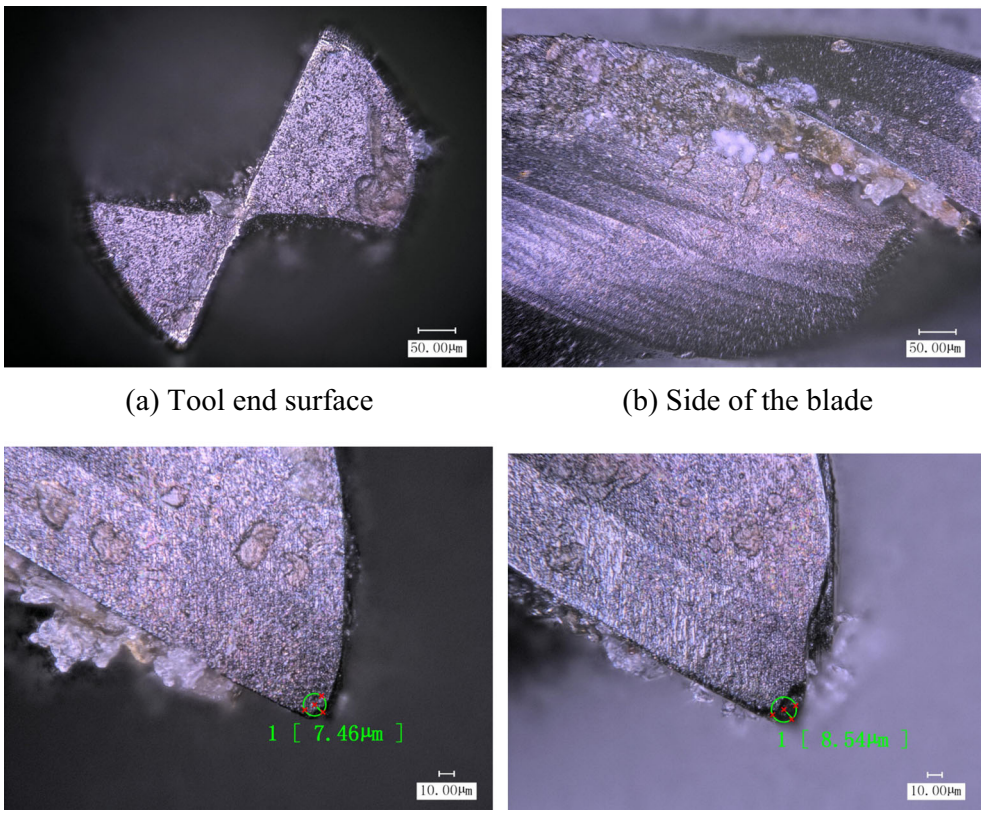

(a) Tool end surface (b) Side of the blade

(c) Measurement of blade 1# (d) Measurement of blade 2#

Fig. 18 Corner radius measurement of the micro-milling tool

From the observation of the results, the top burr size variation has two parts. The burr size steadily and quickly increases in part 1, when f is 0–1.5 μm, and the top burr size first decreases and subsequently slowly increases in part two, when f is greater than 1.5 μm. When f is below the minimum chip thickness h_m, normal chip formation and growth are restrained. Large squeezing and tearing of a material result in a poor machined surface. A linear relationship between f and b_l is revealed. However, the top burr width b_w does not exhibit this character. The top burr formation on the micro-milling slot is severe and difficult to control. The method that this study developed can only have a limited minimization, although both burr length b_l and burr width b_w are reduced by greater than approximately 70 %.

On the contrary, when f is above the minimum chip thickness h_m, the chip formation is smooth and regular. The top burr size of uncoated results also presents a decline in this range. Moreover, the minimization effect of the new method achieves the best result, where there is almost no top burr on the micro-milling sides (both up- and down-milling sides), as shown in Figs. 19 and 20.

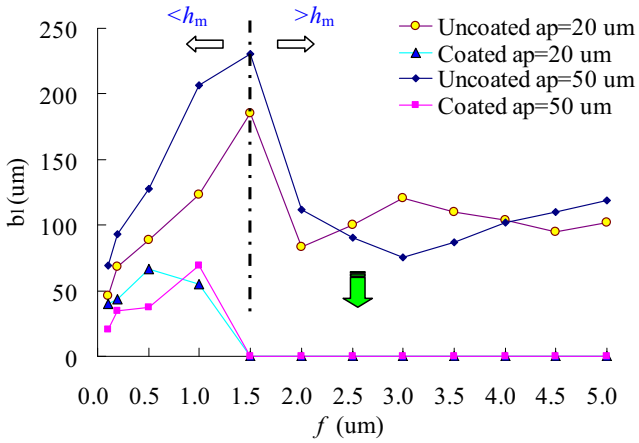

(a) Burr length b_l

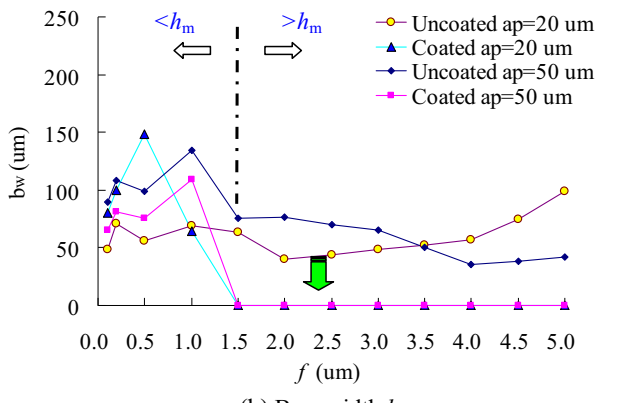

(b) Burr width b_w

Fig. 19 Top burr size on the up-milling side

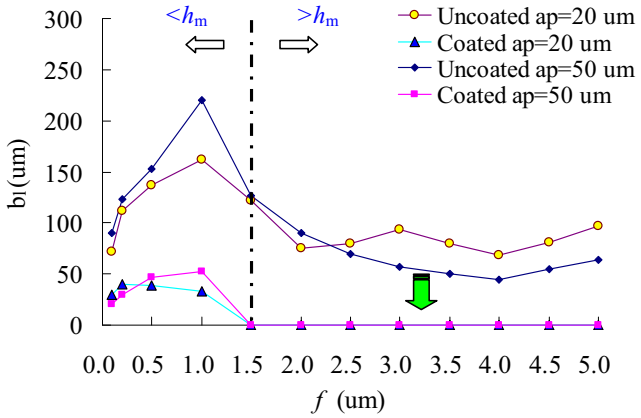

(a) Burr length b_l

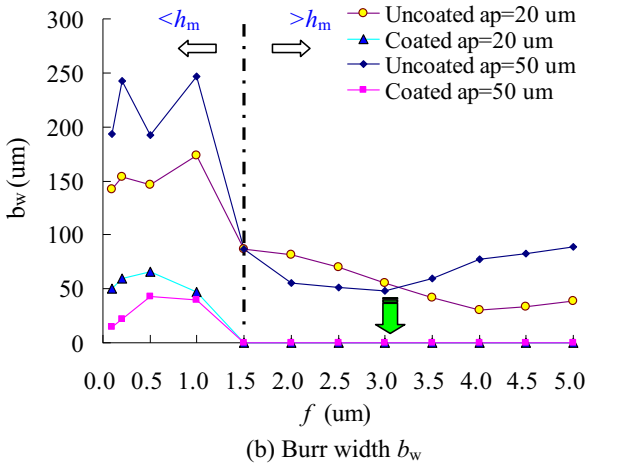

(b) Burr width b_w

Fig. 20 Top burr size on the down-milling side

The result analysis of Figs. 19 and 20 shows that the feed per tooth f is the most important factor for the top burr size. The axial cutting depth a_p does not show a regular effect on the top burr width b_w and top burr length b_l. However, the peak point comparison of top burr size indicates that a larger top burr tends to occur at large a_p.

4.5 Effect of the cutting force work on the top burr size

Figure 21 shows the relation between the top burr size and the cutting force work W_p when a_p is 20 μm. The results on the curve show that both burr length b_l and burr width b_w suddenly change when h is below h_m. In this range, this study supposes that the scrape and plough effects of the material removal mode induce larger W_p into the top burr formation. Meanwhile, relatively larger-size top burrs occur and can be observed on the micro-end milling side. Figure 22 shows the results when a_p is 50 μm, which also shows the identical phenomenon.

Figures 21 and 22 also present the mathematical expression of the top burr size variation versus W_p with

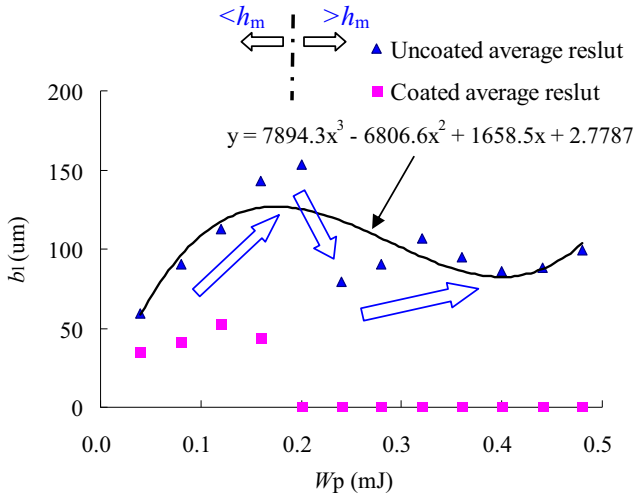

(a) Burr length b_l

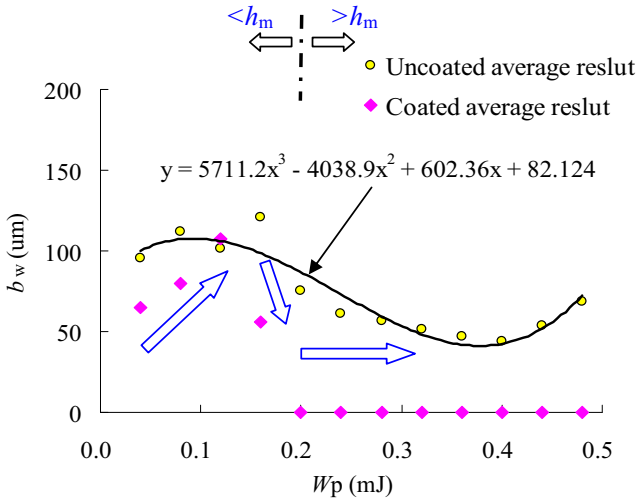

(b) Burr width b_w

Fig. 21 Top burr size versus W_p ($a_p = 20$ μm)

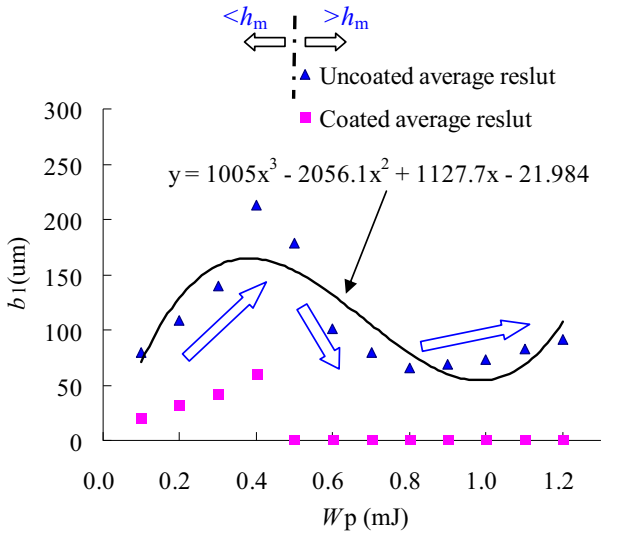

(a) Burr length b_l

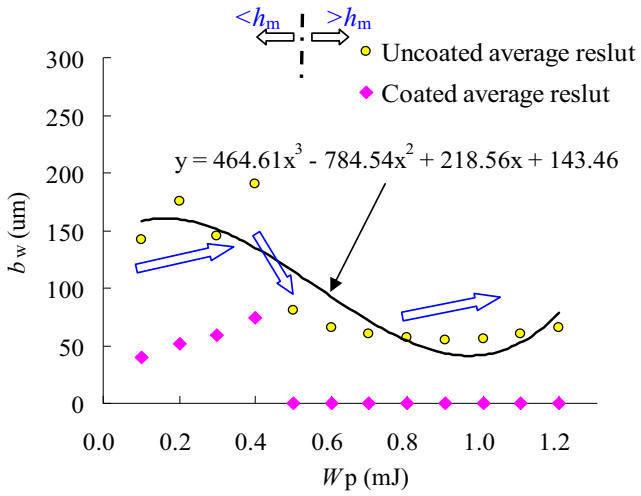

(b) Burr width b_w

Fig. 22 Top burr size versus W_p ($a_p = 50$ μm)

different axial cutting depths a_p. The polynomial expressions of the relationship are fitted in this study. From the results in Figs. 21 and 22, it can be deduced that the top burr size usually increases with the micro-milling force and force work W_p, whereas the machining quality and precision decrease with the increase in micro-milling force. However, under different material removal modes, the variation in the machining results has different relations to the cutting force. At the micro-machining range, the most obvious phenomenon is that the relation shows significant differences at two sides of the minimum chip thickness.

Based on those results, models to predict the top burr size in Eqs. (15)–(18), which this study builds, were solved. The coefficients in these equations were solved based on experimental results and are listed in Table 4.

Evidently, the top burr formation minimization method that this study proposes for the micro-milling of Ti-6Al-4V is significantly effective. Moreover, unlike the available deburring technologies, this new method does not induce any material removal or harmful treatment to the machined surface, which is notably important for the micro-machining of micro-components.

Table 4 Coefficients in the top burr model for the micro-end milling of Ti-6Al-4V

a_p (μm)	k	b_{cu} (μm)	b_{cd} (μm)	$b_{cu\text{-}coating}$ (μm)	$b_{cd\text{-}coating}$ (μm)
20	15,476	12.68	41.96	−28.51	−3.27
50	23,053	0.61	31.18	−112.76	−74.59

5 Conclusions

A new top burr minimization method was proposed and successfully developed in this study for the micro-end milling of Ti-6Al-4V, and the following conclusions are drawn from the results of this study:

1. A top burr formation model was built considering the work of F_p along the chip thickness direction (W_p).
2. The top burr minimization technology that this study develops was verified using a series of micro-end milling experiments of Ti-6Al-4V. The top burr sizes were measured and proven to significantly decrease.
3. The effect of the minimum chip thickness h_m on the top burr formation was investigated in this study. Two different top burr formation modes during the micro-end milling of Ti-6Al-4V have been revealed.
4. The relation between top burr size and cutting force work W_p was discussed. The mathematical expressions of the variation in top burr size versus W_p with different axial cutting depths a_p were presented.

Using the new technology that this study develops, a series of micro-milling surfaces were achieved with the smallest top burr size worldwide to date. The knowledge that this study presents will be an important contribution to minimizing top burr in the micro-end milling of Ti-6Al-4V.

References

1. Peters M, Leyens C (2003) Titanium and titanium alloys. Fundamentals and applications. Wiley-VCH, Weinheim
2. Ezugwu EU, Wang ZM (1979) Titanium alloys and their machinablity—a review. J Mater Process Technol 68:262–274
3. Aurich JC, Haberland R, Schuler GM, Engmann J (2008) A new approach for using micro-end mills at high rotational speed and ultra low run-out, Proceedings of the 3rd International Conference on High Performance Cutting, Dublin, pp 189–197
4. Gillespie LK (1999) Deburring and edge finishing handbook. SME, Michigan
5. Dornfeld D, Min S, Takeuchi Y (2006) Recent advances in mechanical micromachining. Ann CIRP 255:745–768
6. Lai X, Liu H, Li C, Lin Z, Ni J (2008) Modelling and analysis of micro scale milling considering size effect, micro cutter edge radius and minimum chip thickness. Int J Mach Tools Manuf 48:1–14
7. Malekian M, Mostofa MG, Park SS, Jun MB (2012) Modeling of minimum uncut chip thickness in micro machining of aluminum. J Mater Process Technol 212:553–559
8. Ding H, Ibrahim R, Cheng K, Chen SJ (2010) Experimental study on machinability improvement of hardened tool steel using two dimensional vibration-assisted micro-end-milling. Int J Mach Tools Manuf 50:1115–1118
9. Gillespie LK (1973) The formation and properties of machining burrs. M.S. Thesis, Utah State University, Logan
10. Schaller T, Bohn L, Mayer J, Schubert K (1999) Microstructure grooves with a width of less than 50 μm cut with ground hard metal micro end mills. Precis Eng 23:229–235
11. Kiha L, Dornfeld DA (2005) Micro-burr formation and minimization through process control. Precis Eng 29:246–252
12. Schuler GM, Engmann J, Marx T, Haberland R, Aurich JC (2010) Burr formation and surface characteristics in micro-end milling of titanium alloys, Proceedings of the CIRP sponsored international conference on burrs: Analysis, Control & Removal, Kaiserslautern, pp 129–138
13. Chern GL (2006) Experimental observation and analysis of burr formation mechanisms in face milling of aluminum alloys. Int J Mach Tools Manuf 46:1517–1525
14. Chern GL, Wu YE, Cheng J, Yao J (2007) Study on burr formation in micro-machining using micro-tools fabricated by micro-EDM. Precis Eng 31:122–129
15. Tang Y, He Z, Lu L, Wang H, Pan MQ (2011) Burr formation in milling cross-connected microchannels with a thin slotting cutter. Precis Eng 35:108–115
16. Piquard R, Acunto AD, Laheurte P, Dudzinski D (2014) Micro-end milling of NiTi biomedical alloys, burr formation and phase transformation. Precis Eng 38(2):356–364
17. Wan ZP, Li YC, Tang HL, Deng WJ, Tang Y (2014) Characteristics and mechanism of top burr formation in slotting microchannels using arrayed thin slotting cutters. Precis Eng 38:28–35
18. Bi SS, Liang J (2011) Experimental studies and optimization of process parameters for burrs in dry drilling of stacked metal materials. Int J Adv Manuf Technol 53(9):867–876
19. Chen MJ, Ni HB, Wang ZJ, Jiang Y (2012) Research on the modeling of burr formation process in micro-ball end milling operation on Ti–6Al–4V. Int J Adv Manuf Technol 62(9):901–912
20. Silva LC, Mota PR, Silva MB, Ezugwu EO, Machado AR (2015) Study of burr behavior in face milling of PH 13-8 Mo stainless steel. CIRP J Manuf Sci Technol 8:34–42
21. Zhang T, Liu ZQ, Xu CH (2013) Influence of size effect on burr formation in micro cutting. Int J Adv Manuf Technol 68(9):1911–1917
22. Wu X, Li L, He N, Zhao M, Zhan ZB (2015) Investigation on the influence of material microstructure on cutting force and bur formation in the micro cutting of copper. Int J Adv Manuf Technol 79(1):321–327
23. Hashimura M, Hassamamontr J, Dornfeld DA (1999) Effect of in-plane exit angle and rake angles on burr height and thickness in face milling operation, transactions of the ASME. J Manuf Sci Eng 121(1):13–19
24. Bissacco G, Hansen H, Chiffre LD (2005) Micromilling of hardened tool steel for mould making applications. J Mater Process Technol 167:2–3